The Use of 3D Xray angiographic Images for Volume Determination of Cerebral Arteriovenous Malformations

Marie-Odile Berger, René Anxionnat, Erwan Kerrien

The Use of 3D Xray angiographic Images for Volume Determination of Cerebral Arteriovenous Malformations

Marie-Odile Berger[a] and René Anxionnat [b] and Erwan Kerrien [a]

[a] Loria Inria Lorraine, BP 101, 54602 Villers les Nancy Cedex, France;
[b]CHU Nancy, 29 av. du Mal de Lattre de Tassigny, 54035 Nancy cedex, France.

ABSTRACT

The radiotherapic treatment of cerebral arterious malformations (AVM) requires an accurate estimation of the AVM shape. This estimation is classically obtained from the delineation of the AVM in several 2D angiographic views. In this paper, a clinical study of the inter-observer variability in the AVM detection is first performed. It proves that the estimated volume varies a lot between observers. For these reasons, we propose a framework for AVM delineation which makes use of 2D and 3D angiographic images: the initial estimate obtained with 2D angiographic images is then refined within the 3D volume using deformable models. Results are presented demonstrating shape delineation on various AVMs.

1. INTRODUCTION

A cerebral arteriovenous malformation (AVM) is defined as a localized arteriovenous shunt consisting of a tangle of capillaries and veins, also called nidus. The treatment of complex AVMs is classically a two stage process. Embolization or endovascular treatment is first performed. It allows to reduce the size of the AVM but is usually not sufficient to cure it completely. This step is then followed by a stereotactic irradiation which consists in a single delivery of a high dose of radiation to the remnant, called *target*, through the intact skull. Therefore, accurate definition of the target is of crucial importance for the efficacy of the treatment. 2D subtraction angiography (2DSA) remains the gold standard for this task: the AVM is delineated in at least two calibrated views and the volume of interest is limited by the intersection of X-ray cones defined by each delineation.[1] However, only a small number of views is allowable because of clinical and technical limitations. This reduces the accuracy of the estimated target. 2DSA can be supplemented by other modalities such as MRI or 3D angiography (3DXA). The challenge here is to define if these modalities are well suited to AVM delineation and to define how to make these modalities cooperate for this purpose. In this paper, we especially considered the use of 3D angiography for AVM delineation. Though 3DXA is used in clinical routine for aneurysms treatment,[2] its relevance for AVM treatment has not yet been studied.

The clinical context of this study is described in section 2. AVM reconstruction from 2DSA is then studied in section 3 and the variability of the reconstructed shape depending on the expert is demonstrated. Using our AVM database and a statistical description of the shape variability, we prove in section 4 that 3DXA is well suited to AVM detection. Finally, we propose in section 5 a framework for the AVM determination which makes use of both 2DSA and 3DXA through the concept of deformable surfaces.

2. CLINICAL CONTEXT

Twelve patients with AVM were treated using embolization and radiotherapy at Nancy University Hospital (France). According to the complexity of the AVM shape, between 2 to 5 2DSA views were considered for delineation (antero-posterior (AP), lateral and oblique views). Overall, 45 2DSA images were available for this study. In addition, the 3DXA volume was available for each patient. Note that these images were acquired in stereotactic conditions, allowing 2DSA/3DXA image registration. The AVMs considered in this study are

Further author information: (Send correspondence to Marie-Odile Berger)
Marie-Odile Berger: E-mail: berger@loria.fr,
Erwan Kerrien: kerrien@loria.fr,
René Anxionnat: r.anxionnat@chu-nancy.fr

Medical Imaging 2004: Physiology, Function, and Structure from Medical Images, edited by Amir A. Amini, Armando Manduca, Proceedings of SPIE Vol. 5369 (SPIE, Bellingham, WA, 2004) · 1605-7422/04/$15 · doi: 10.1117/12.533971

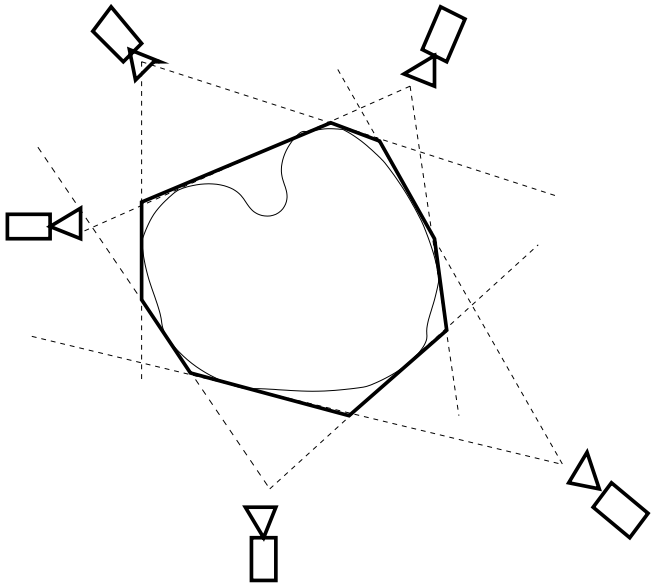

Figure 1. An object and its inferred visual hull.

complex pathological cases. According to the complexity of the delineation task, each AVM was labelled as fairly difficult or very difficult (see table 1).

Five experts in interventional neuroradiology from Nancy University Hospital (France) and Karolinska Institute (Stockholm) were involved in this study. They delineated the AVMs manually on the 45 2DSA images.

3. AVM RECONSTRUCTION FROM DELINEATIONS IN 2DSA

The AVM shape was computed as the intersection of the 3D cones defined by each delineation in the calibrated 2DSA. In fact, we only computed the *visual hull* of the shape[3] which is an approximation of the true shape (Fig. 1). This visual hull is guaranteed to enclose the object and its size decreases monotonically with the number of images used. Here, the method of Szeliski[4] was used for computing the visual hull because it allows significant increase in processing speed. Though classically used for volumetric scene reconstruction from photographs, this method only provides a rough approximation of the shape in our context:

- Only a small number of views is available (from 2 to 5 views). Hence, depending on the viewpoints, some parts of the reconstructed shape can be far from the actual shape. Moreover, not all concavities can be modeled with the visual hull.
- The delineation of an AVM is a difficult task: this can be straightforward on a small compact nidus and very difficult in a previously embolized patient or when some parts of the boundary are hidden by vessels superposition. Such difficulties prevent from delineating the true boundary and lead to inaccurate reconstruction.

Let us consider the case of patient 1, tagged as fairly difficult by the experts. Three views were considered: AP, lateral and one oblique view (Fig. 2:a,b and c). The superimposition of the expert curves on the three views clearly proves that the opinion of the experts can considerably differ. Of course, this induces large variability on the reconstructed shape for each expert. Table. 1 provides for each patient, the volume of the reconstructed shape for each expert.

In addition, this example clearly shows that the delineations of the AVM in each view are not consistent (Fig. 2:e,f,g): the backprojection (in black) of the reconstructed shape in the view does not match the original delineation of the expert (in white).

Patient	AVM difficulty	Expert1	Expert 2	Expert 3	Expert 4	Expert 5	Mean	Deviation
1	fair	3.47	2.54	2.13	2.16	0.91	2.24	0.82
2	fair	1.92	1.58	0.88	1.44	0.99	1.36	0.38
3	difficult	11.25	5.42	8.17	5.84	3.47	6.83	2.66
4	fair	13.29	13.50	14.04	15.10	9.33	13.05	1.96
5	difficult	8.21	6.82	4.62	3.71	2.87	5.25	1.98
6	fair	8.45	7.40	6.88	7.76	2.92	6.68	1.95
7	difficult	14.34	13.23	8.25	13.37	5.30	10.90	3.51
8	difficult	7.04	10.99	12.20	14.28	4.11	9.72	3.66
9	difficult	7.82	2.65	4.85	3.66	3.23	4.44	1.83
10	fair	0.80	1.28	0.71	0.55	0.70	0. 81	0.25
11	difficult	0.75	0.53	0.39	0.47	0.24	0.48	0.17
12	difficult	3.81	4.95	4.90	4.98	2.12	4.15	1.11

Table 1. The inter-observer variability in the estimated volume of the AVM. Volumes are expressed in cm^3.

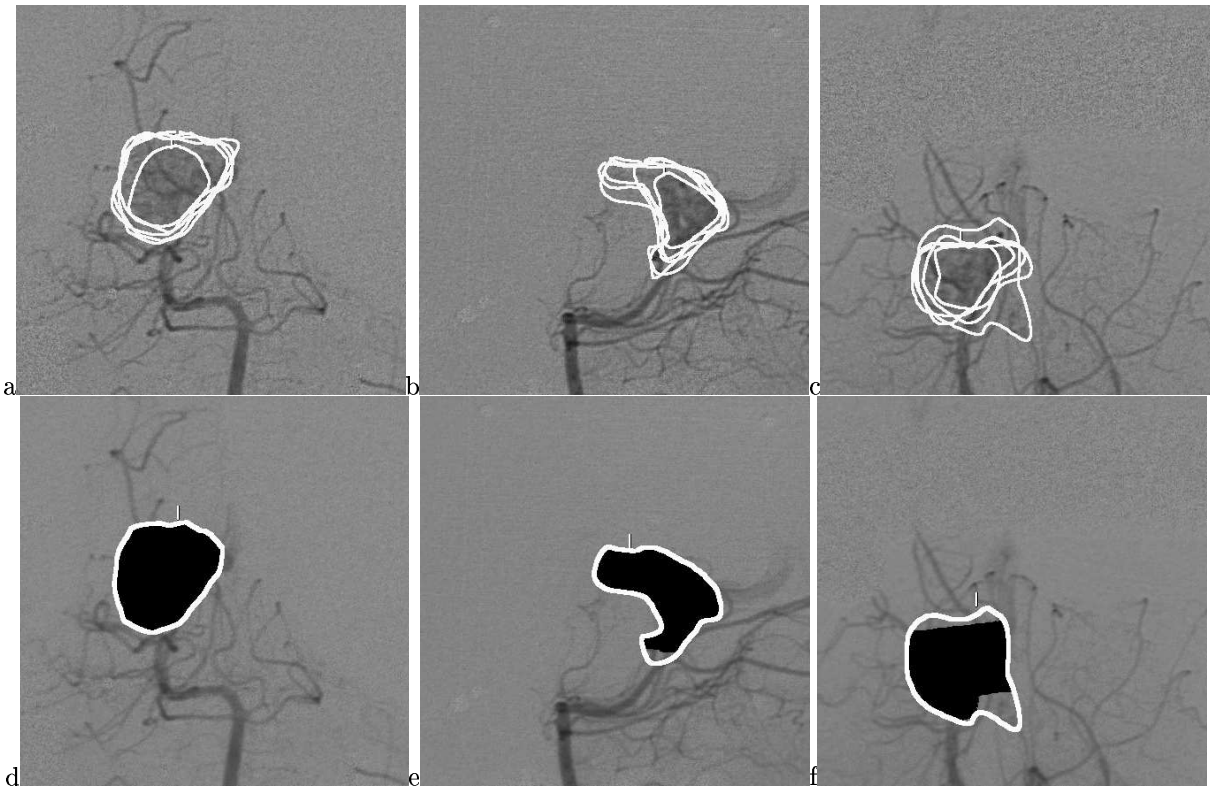

Figure 2. AVM delineation from 2D angiographic views.
First raw:Variability in expert delineations on the antero-posterior, lateral and oblique views.
Second raw: Delineation of the expert (curve in white) and backprojection of the reconstructed shape in each angiography (in black).

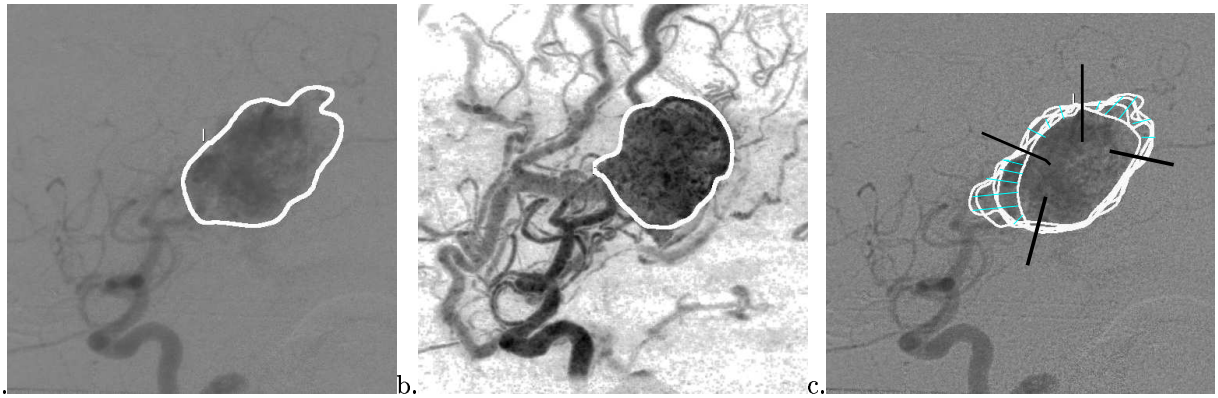

Figure 3. Delineation on 2DSA (a) and MIP (b) images. Semi-automatic curve reparameterization.

Though 2DSA is considered as the gold standard for patient delineation, this study proved that delineations vary considerably between observers and lead to considerable variation in shape reconstruction. It appeared that this estimated volume should not be used for radiotherapy planning but should rather be considered as a first estimate of the shape, to be refined using another available modality.

4. ASSESSMENT OF 3DXA FOR AVM DELINEATION

Due to the considerable variability in the reconstructed shape, we investigated the possibility to use 3DXA images to refine the AVM shape. This refinement can be considered in two ways: (i) 3DXA volume allows us to generate virtual 2D views without further dose exposure for the patient. These views are more general than the classical 2D views: not all orientations are reachable by the angiography machine whereas Maximum Intensity Projection views (MIP) of the 3DXA volume can be generated for any position. Hence, the physician could potentially use an arbitrary number of views to delineate the AVM. (ii) 3DXA volume can also be used to refine the first estimate directly in 3D. We investigate this strategy in section 5.

However, before using 3DXA, we have to assess if this modality is well suited to AVM detection. Indeed, nidus are identified from the arterial phase, just as the draining vein begins to fill. As 3DXA volume is an averaged image acquired during the whole progression of the opaque mixture, it is not clear if it will allow nidus detection.

4.1. Method

In order to prove the interest of using 3DXA in AVM delineation, the following set up was used. For each patient, the MIP images of the 3DXA were computed with the same viewing parameters used for the acquisition of 2DSA images. Then, all the experts delineated the AVM in these MIP views. Fig. 3 exhibits two delineations by the same expert on the 2DSA and the MIP images. Assuming that the delineations by the experts on 2DSA are the gold standard we have to determine if the delineations stemming from the 3DXA can be considered as an instance of the model provided by delineations in 2DSA.

To deal with variations in appearance of delineations, we used statistical models derived from the set of expert curves on 2DSA. To this aim, dense correspondences between shape boundaries were established using a semi-interactive interface: all the boundaries were displayed and a physician drew linear cuts (Fig. 3.c). Reparameterization of the boundaries was performed in a piecewise manner between two consecutive cuts. In practice, segments were defined to limit the consensus areas between experts.

Let $x_{i\{1\leq i\leq N\}}$ be the set of curves delineated by the experts, where N is the number of experts. Let $\bar{x} = \frac{1}{N}\sum_{i=1}^{i=N} x_i$ be the mean of the curves, computed from point-to-point correspondences, and $S = \frac{1}{N-1}\sum(x_i - \bar{x})(x_i - \bar{x})^t$ be the covariance of the data. Following Cootes,[5] a linear eigen-model can be built by applying a

principal component analysis (PCA) to obtain the t principal modes of variation represented by the $N \times t$ matrix P of eigenvectors of S corresponding to the t largest eigenvalues. A particular patch x is then approximated by

$$x \approx x' = \bar{x} + Pb$$

where

$$b = P^t(x - \bar{x}).$$

The error on this approximation is therefore

$$r^2 = ||x - x'||^2 = (x - \bar{x})^t(x - \bar{x}) - b^t b.$$

The value of t is chosen so that the model represents a suitable proportion of the variation in the training set (95%).

4.2. Quality of fit measures

We are interested in deciding how a new delineation matches the model. A first measure of the quality of fit is classically deduced from the PCA:

$$fit_1(x) = \sum_{i=1}^{i=t} \frac{b_i^2}{\lambda_i}$$

where λ_i is the i-th largest eigenvalue in the PCA and $b = (b_i)$. This value only measures the distance of the shape from the mean along the modes of the model but it does not consider the distance of the delineation from the linear model $r^2 = (x - \bar{x})^t(x - \bar{x}) - b^t b$. We have to define a measure to decide if the residual r is compatible with the expert database. To this aim, we resort to cross-validation : an expert curve is left out at a time; the PCA is performed on the remaining data; and the generalized error is estimated as the average of the residuals for the removed expert curves. Hence a good way to assess a delineation x is to consider

$$fit_2(x) = \frac{\sum_{expert} r^2_{expert}(x)}{\sum_{expert} r^2_{expert}(expert)}$$

where $r^2_{expert}(x)$ is the PCA residual when the curve of the *expert* is left out.

The entire measure of fit is then defined as the sum $fit(x) = fit_1(x) + fit_2(x)$.

4.3. Results

In order to design a statistical test for acceptation/rejection of new delineations, the distribution of the fit measure must be studied. Fig.4 shows the distribution of the fit measure when all the patients are considered. This histogram is performed in a miss-one-out manner to densify the data. The shape of this histogram suggests that the fit measure is distributed approximately as a χ square. As the number of independent principal components is $t = 3$ in our application, and if we consider errors r as Gaussian, the degree of freedom, is at most 4. However r and the principal components are not independent. In practice, according to Fig.4 which superimposed $\chi^2(3)$ (with bold lines) and $\chi^2(4)$ (with dotted lines) on the histogram, we consider that the distribution of fit can be modeled with a χ square distribution with 3 degrees of freedom. It must be noted that with a slightly different term fit_2,[5] found experimentally on a particular application that $t+1$ gives a reasonable estimation of the number of degrees of freedom.

In order to assess the relevance of 3DXA, each delineation on the MIP images was tested using the fit measure. If we consider the complete set of AVMs, 65% of the MIP curves were accepted by the statistical test. If we restrict our study to fairly difficult AVMs, the acceptation rate is 85%. These results must be compared to the acceptation rate of each expert curve on classical 2DSA images when compared to the statistical model built from the other experts. The mean acceptation rate is 72% but this rate varies a lot between the experts: the best acceptation rate is 95% and the worse 50%.

If we consider the high variability between the experts and the acceptation rates obtained with MIP views, especially for fairly difficult AVMs, this study proves that the 3DXA volumes can be used for AVMs delineation.

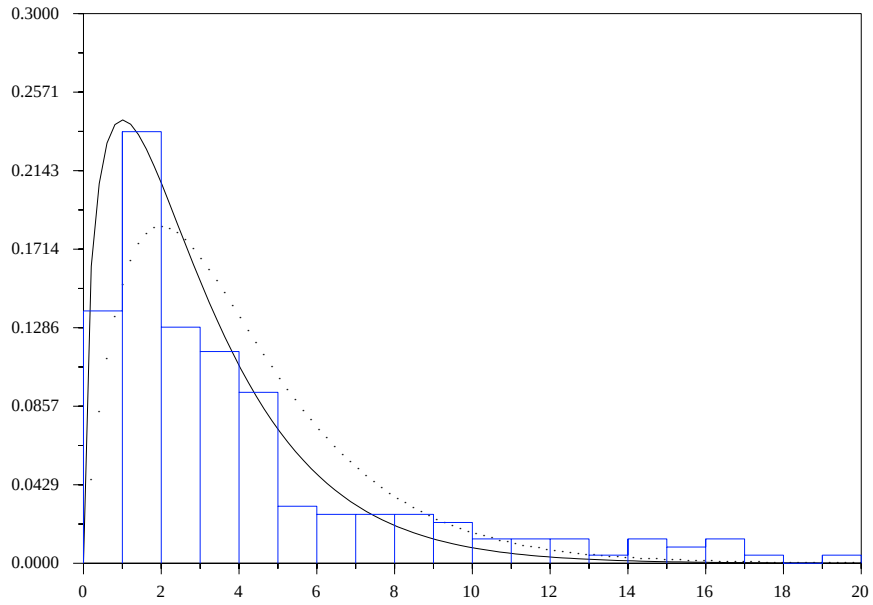

Figure 4. Histogram of the fit values as well as the curves $\chi^2(3)$ (bold line) and $\chi^2(4)$ (dotted line).

5. ACTIVE SURFACES FOR AVM REFINEMENT

Though inaccurate, the shape reconstructed from delineations in 2DSA images is a first estimate for the location and shape of the AVM. It is then natural to resort to deformable surfaces to refine the AVM shape from this initial guess. The widely recognized potency of deformable models in medical imaging[6] stems from their ability to segment, match and track images of anatomic structures by exploiting constraints derived from the image data together with a priori knowledge about the location, size and shape of these structures.

Deformable models have various formulations : explicit representation form, implicit form[7] and mesh representations.[8,9] For mesh representation, deformation is performed by constraining the model directly on its vertices. Besides the classical advantages of mesh representation: simplicity, speed and fast rendering, we used this representation for the following reasons (i) As the shape of the AVM can be complex, mesh representation permits a large number of degrees of freedom for the surface (ii) Constraints on the allowable deformations can be easily added (iii) Topological adaptation of the shape at each step is possible and allows complex shapes to be handled.[9]

5.1. Method

In our method, a first estimate of the AVMS volume is computed from 2D delineations. The surface of the AVM is then extracted thanks to a marching-cube algorithm. As a result, we get a triangulated mesh whose vertices are denoted by X. The Newton law of motion is applied on each vertex:

$$m\frac{d^2X}{dt} + \gamma\frac{dX}{dt} = f_{internal}(X) + f_{external}(X)$$

The internal forces are classically defined as[9]:

$$f_{internal}(X) = \alpha(\bar{X} - X) + \beta \sum_{Y \in N(X)} (||Y - X|| - l) \frac{Y - X}{||Y - X||}$$

where $\bar{X}$ is the mean of all the neighbors of X, $N(X)$ is the set of neighbors of X, and l is the edge rest length for the whole mesh. l can be set to the average of all edge lengths to regularize them along the entire mesh.

We now have to define the data forces that are applied on the surface. Image criteria for AVM detection on 2D angiography seem to be difficult to define, maybe due to the superposition of vessels in projection. Fortunately, gradient based criteria seem to be well suited to the AVM structure in 3D because the AVM appears as a nidus of vessels with relatively high gradient. Hence we used a classical external term $f_{external}(X) = \nabla||\nabla(G_\sigma \star I(X)||$, where the intensity I in the 3DXA volume is smoothed with a Gaussian kernel. The evolution equation is solved iteratively using a semi implicit scheme.

5.2. Results

In this section, examples of AVM detection are shown. Fig.5 and Fig.6 are examples of fairly difficult AVMs which correspond to patient 1 and 4. Four 2DSA views were available. First, an estimate of the AVM volume was built from these views using cone intersection. Fig.5 exhibits the intersection of the shape with several slices of the 3DXA volume (first raw). Then, deformable surfaces were used from this initial estimate. The resulting mesh is shown on the second raw on the same slices. Finally, the reconstructed AVM is shown in Fig.5.a with its back-projection on 2DSA views. The visual impression of the obtained volume onto the 3DXA is good. The use of deformable surfaces seems to greatly improve the detection of the AVMs. A medical expert confirmed the pertinence of the AVM delineation in 3DXA.

For these patients, we also tested if the estimated shape matched the model of the experts. To do this, we used the statistical test described in section 3. For patient 1 (Fig. 5), the projection of the AVM on the 2DSA images was accepted for all the views. For patient 4 (Fig.6), the AVM was accepted on two views and rejected (but just above the acceptation threshold) for the other two. One of these rejected curves is shown in Fig.6.c. It must be noted that when a $\chi^2(4)$ distribution was used instead of a $\chi^2(3)$, all the views were accepted.

6. CONCLUSION AND DISCUSSION

The contributions of this paper are twofold. On a clinical point of view, our clinical study shows that volume determination of the AVM from delineations on 2DSA views varies considerably according to the observer. These variability can be easily explained by the difficulty to detect the AVM boundary due to vessel superposition. This study questions whether considering 2DSA images as gold standard is still appropriate for AVM delineation. We also proposed in this paper a complete method for AVM delineation which makes use of both 2D and 3D angiographic images. These two modalities complement themselves because 2D images allow the AVM to be roughly located whereas AVM detection in 3D alone may be difficult or even impossible (AVM with fast blood flow). Fortunately, we showed that 3DXA images can be used to refine the AVM shape. Our experiments proved the reliability of the method on several significant examples. We now plan to test this method on a large range of patients. These tests aim at studying the influence of the form of the image force on the results as well as the influence of the numeric parameters of the deformable models. Finally we want to complement this framework with the use of MRI images.

REFERENCES

1. M. Soderman, B. Karlsson, L. Launay, B. Thuresson, and K. Ericson, "Volume measurement of cerebral arteriovenous malformatios from angiography," *Neuroradiology* **42**, pp. 697–702, 2000.
2. R. Anxionnat, S. Bracard, X. Ducrocq, Y. Trousset, L. Launay, E. Kerrien, M. Braun, R. Vaillant, F. Scomazzoni, A. Lebedinsky, and L. Picard, "Intracranial aneurysms: Clinical value of 3d digital subtraction angiography in the therapeutic decision and endovascular treatment," *Radiology* , pp. 799–808, Mar 2001.

3. A. Laurentini, "How Far 3D Shapes Can Be Understood from 2D silhouettes," *IEEE Transactions on PAMI* **17**, pp. 188–195, Feb. 1995.
4. R. Szeliski, "Rapid Octree Construction from Image Sequences," *CVGIP: Image Understanding* **58**, pp. 23–32, July 1993.
5. T. Cootes, C. Page, C. Jackson, and C. Taylor, "Statistical grey-level models for object location and identification," *Image and Vision Computing* **14**, pp. 533–540, 1996.
6. T. McInerney and D. Terzopoulos, "Deformable models in medical images analysis: a survey," *Medical Images Analysis* **1**(2), 1996.
7. R. Malladi, J. Sethian, and B. Vemuri, "Shape Modeling with Front Propagation: A level Set Approach," *IEEE Transactions on PAMI* **2**(17), pp. 158–175, 1995.
8. H. Delingette, "Simplex meshes: a general representation for 3D shape reconstruction," in *Conf. on Computer Vision and Pattern Recognition (CVPR '94)*, June 1994.
9. J.-O. Lachaud and A. Montanvert, "Deformable meshes with automated topology changes for coarse-to-fine 3D surface extraction," *Medical Image Analysis* **3**(2), pp. 187–207, 1999.

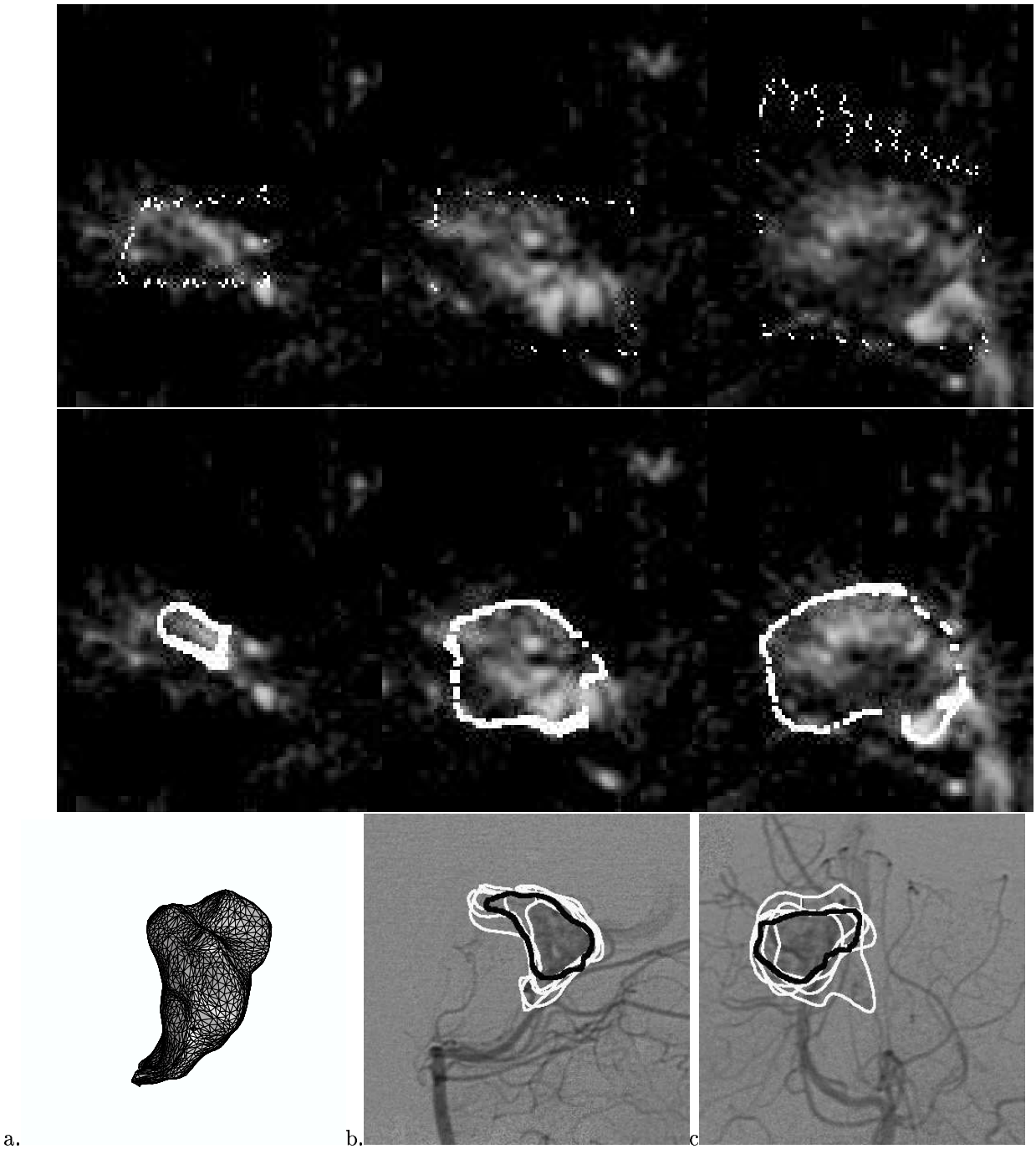

Figure 5. AVM refinement after the use of active surfaces (patient 1).
First raw: superimposition of the initial AVM volume on several slices
Second raw: superimposition of the AVM volume after the use of deformable surfaces.
Third raw: (a) the 3D shape of the AVM (b and c): backprojection of the estimated AVM onto a lateral and an oblique view.

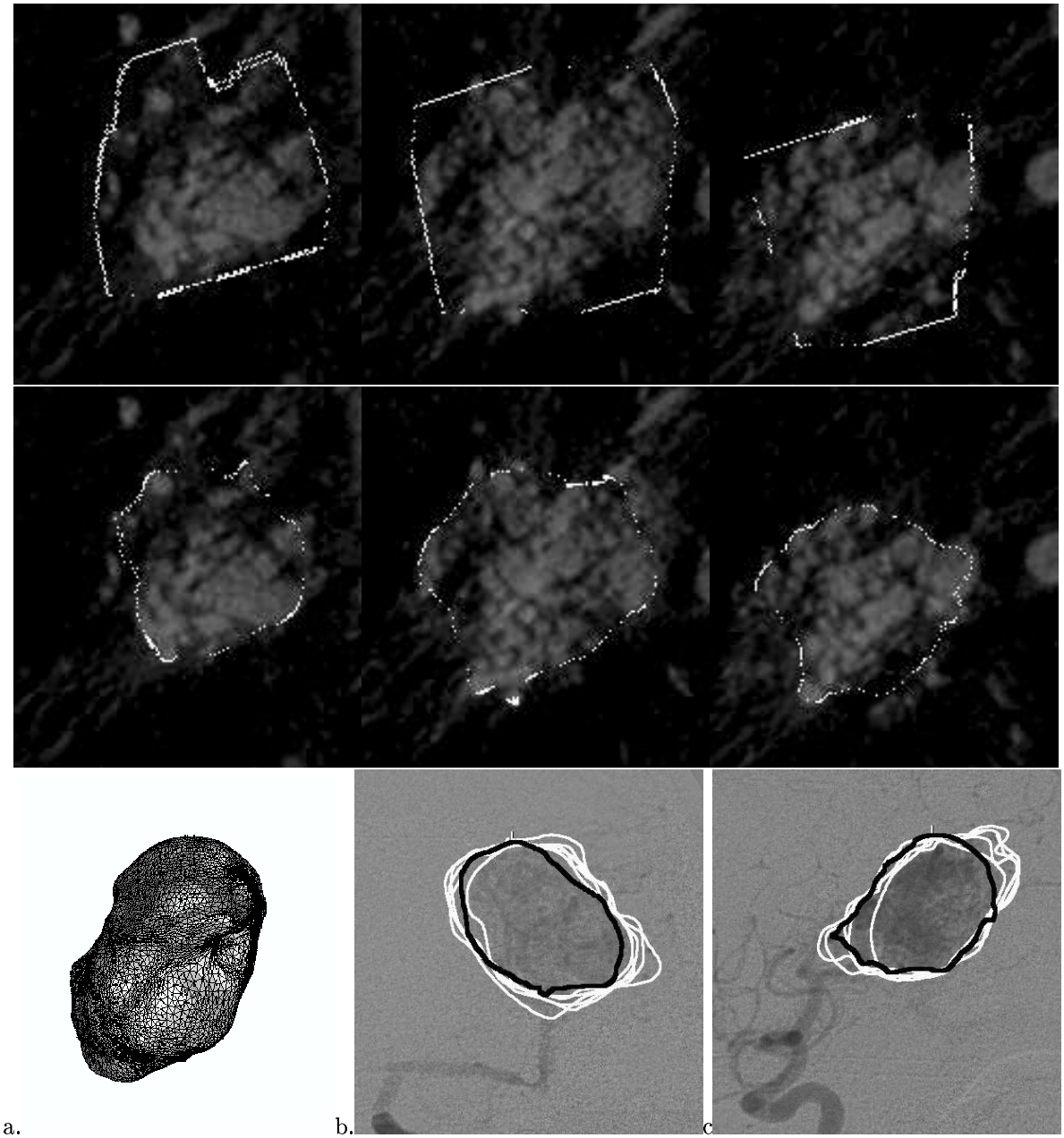

Figure 6. AVM refinement after the use of active surfaces (patient 4).
First raw: superimposition of the initial AVM volume on several slices
Second raw: superimposition of the AVM volume after the use of deformable surfaces.
Third raw: (a) the 3D shape of the AVM (b and c): backprojection of the estimated AVM onto the antero-posterior and lateral views.